J Mater Sci (2007) 42:5135–5141
DOI 10.1007/s10853-006-1265-3

Characterization of carbon coatings on SiC monofilaments using Raman spectroscopy

Yanling Ward · Robert J. Young · Robert A. Shatwell

Received: 22 July 2006 / Accepted: 13 November 2006 / Published online: 26 April 2007

Abstract The axial residual stresses in the carbon coatings deposited onto different silicon carbide monofilaments have been determined experimentally using Raman spectroscopy. The stress-dependent band shift for the carbon G-band at around 1600 cm^{-1}, due to symmetric in-plane stretching mode of graphite, has been found to be –1.6 cm^{-1}/GPa. Using this calibration, the axial residual stresses in carbon coatings can be estimated from measured band shifts between the broken end and middle of the monofilaments. It was found that the stresses in the coatings of all monofilaments were compressive and between –440 and –810 MPa. Modelling indicated that this was consistent with the coating stress arising from the difference in coefficients of thermal expansion of carbon and the underlying silicon carbide. The coating stress was measured as a function of distance from the broken monofilament end. It was found that the distance for the stress to build up varied greatly, from 40 μm in Ultra-SCS to 500 μm in SM1140+. This suggests there are significantly different shear stresses between the coatings and underlying silicon carbide in the different monofilaments.

Introduction

Large diameter SiC monofilaments produced by the CVD process have been developed as reinforcements for metal- and ceramic-matrix composites. They have high strength, high modulus and excellent thermal stability. These SiC monofilaments are usually deposited with an approximately 3–5 μm thick carbon coating before incorporated into composite materials. Such a coating protects the SiC monofilament from surface damage and consequently improves its mechanical strength. It also plays an important role in controlling the interface with the matrix. However, deposition of such coatings at high processing temperatures also results in the development of large thermal residual stresses due to thermal mismatch between the coating and the SiC substrate [1, 2]. The presence of excessive coating compressive stresses could easily lead to extensive debonding at the interface [1] and a tensile coating stress could lead to cracking [2]. Determination of the residual stresses is therefore important for the improvement of the coating process to achieve better performance of both the monofilaments and the composites.

Previous studies [1, 3, 4] have shown that surface coating on most of the SiC monofilaments consists mainly of carbon. X-ray diffraction and neutron diffraction data come from the bulk of the monofilaments as a whole, and are also more sensitive to silicon carbide than carbon. Since the penetration depth of the laser beam into carbon is less than 0.1 μm, Raman spectroscopy can only detect signals from the surface of a monofilament. It is therefore suitable for studying surface coatings on the SiC monofilaments. Raman spectroscopy is a sensitive method for identifying different forms of carbon [5–9], as well as characterizing structural perfection and ordering in carbon, graphite and carbon fibres [5–13]. It has also been shown to be a non-destructive technique for monitoring stress and strain in graphite and carbon fibres [10–13], and carbon-containing SiC fibres produced by polymer precursors [14, 15]. Recently we have demonstrated that the technique developed for the deformation studies of carbon fibres can be extended effectively to the study of deformation

Y. Ward · R. J. Young (✉) · R. A. Shatwell
Materials Science Centre, School of Materials, The University of Manchester, Manchester M1 7HS, UK
e-mail: robert.young@manchester.ac.uk

behaviour of CVD-type SiC monofilaments, by following the shifts of carbon bands from the carbon coatings on the monofilaments [16]. In this paper it is demonstrated how Raman spectroscopy can be used to estimate the residual stresses in the coatings of different SiC monofilaments. The technique has also been used to determine stress distribution away from the broken ends along the monofilaments so that the interfacial adhesion and mechanism of stress transfer between the coating and the underlying silicon carbide can be investigated.

Experimental

Materials

The SiC monofilaments used in this study had either tungsten or carbon cores. The tungsten-cored samples were made by QinetiQ (Farnborough, UK). They consisted of a standard, 105 μm diameter SM1140+ monofilament and two experimental ~140 μm diameter samples, denoted here as samples A and B. The carbon-cored monofilaments were SCS-6 and Ultra-SCS, supplied by SMI (Lowell, USA) and had diameters of ~140 μm. The relevant physical and mechanical properties of the SiC monofilaments examined in this study are given in Table 1.

Tungsten-cored SiC monofilaments were grown by chemical vapour deposition using a two-stage process. A mixture of dichloromethylsilane (DCMS) and hydrogen was first reacted at the surface of an electrically heated tungsten wire (15 μm diameter) to produce a SiC monofilament. A ~5 μm thick carbon coating was then deposited onto the SiC substrate in a separate reactor from a mixture of propane and chloroform in argon at approximately 1000 °C.

The carbon-cored SiC monofilaments were grown in a two stage process on a ~33 μm carbon core heated at 1200–1400 °C, from a gas mixture of chlorosilane and hydrogen. The ~3 μm carbon coating was produced at the bottom of the second reactor from a mixture of propane, chlorosilane and argon.

Table 1 Material and mechanical properties of the SiC monofilaments

Monofilaments	Fibre diameter (μm)	Coating thickness (μm)	Young's modulus (GPa)	Fracture strength (GPa)
SCS-6	140	3	390	4.4
Ultra-SCS	143	3.3	410	5.6
SM1140+	110	4	380	3.3
A	138	3	400	4.1
B	140	3	400	N/a

Raman spectroscopy

All the Raman spectra were obtained from a Renishaw 1000 Raman system using the 633 nm line of a He–Ne laser and a sensitive Peltier-cooled coupled charge device (CCD) detector. The laser beam was focused on the sample using a 50× objective lens. The laser polarization was parallel to the axial direction of monofilaments in all measurements. It has been reported previously [14] that a high laser power (>50 mW) and long exposure time causes downshifts of both carbon bands, as a result of overheating induced at the sample surface. In our experiments, Raman spectra were obtained with laser powers less than 2 mW and exposure times of less than 60 s to avoid this effect. A neon lamp was introduced into the system and its 1582.5 cm^{-1} line was used as an internal calibration for the spectra. All the spectra were curve fitted using GRAMS curve-fitting software as discussed elsewhere [16].

Results and discussion

Microstructure of the surface coatings

Figure 1 shows the Raman spectra obtained from the coating surface of the monofilaments in the 300–2000 cm^{-1} region. The spectra resemble those of disordered graphite [9, 13] and low-modulus carbon fibres [9, 13], showing two broad overlapping bands at around 1300 and 1600 cm^{-1}. The G-band at 1600 cm^{-1} is assigned to the E_{2g} symmetry in-plane stretching mode of single crystal graphite, and the D-band at 1330 cm^{-1} is attributed to the breathing mode of A_{1g} symmetry, which only becomes active in the presence of disorder arising from the crystal boundaries of polycrystalline graphite [5–9]. The presence of carbon bands in the Raman spectra indicates the existence of carbon in the surface coatings of all monofilaments.

The appearance of the Raman spectra, i.e. position, width, and intensity of both carbon bands, is sensitive to the structural disorder in the carbon structure. Any differences in the Raman bandshape of both carbon bands reflect changes in the microstructure of carbon. It is, therefore important to know the curve fitting procedures used when comparing band positions and bandwidths. Since the carbon Raman bands from carbon coating are overlapping and rather broad, the determination of band position and bandwidth could be affected by the curve fitting procedure used, such as the number of bands chosen and particular function used to fit the band. Due to the asymmetrical nature of the G-band with tails towards lower wavenumber,

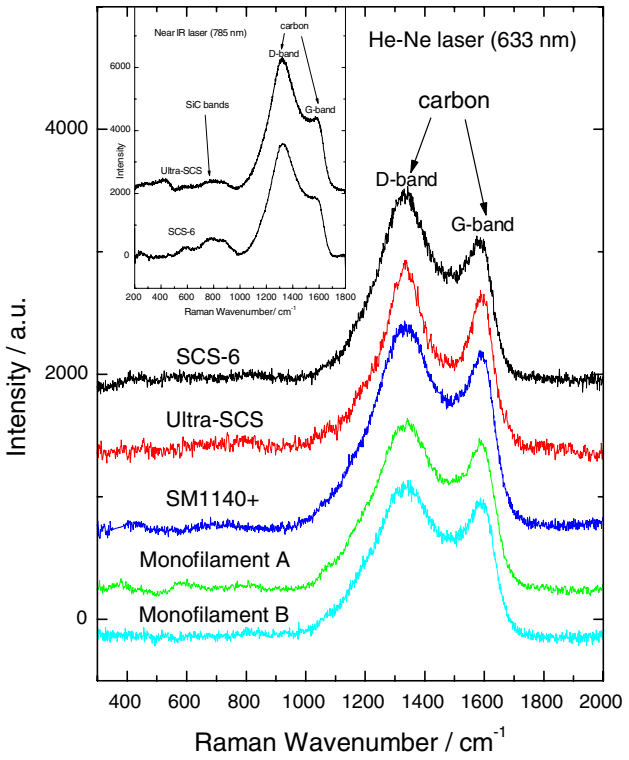

Fig. 1 Raman spectra in the range 300–2000 cm^{-1} obtained from the surfaces of various coated SiC monofilaments, showing both D- and G-bands characteristic of carbon at 1330 and 1600 cm^{-1}

it is often necessary to add more bands to get best fit of the whole spectrum. The carbon spectrum has been fitted by a Lorentzian for the D-band and two Gaussians at ~1500 and 1600 cm^{-1} for the asymmetrical G-band [14], while others [8] tried a Lorentzian fit for the D-band and an asymmetrical Breit–Wigner–Fano (BWF) fit for the G-band. In the present study we have chosen to fit the D-and G-bands separately using a Lorentzian function on a linear sloping baseline, consistent with previous studies [13, 16]. It has been shown that the D-band grows in intensity with increasing disorder or decreasing crystal size and the ratio of its intensity to that of G-band, I_D/I_G, is inversely proportional to the average in-plane crystallite size (L_α) for disordered graphite in the range 2 nm< L_α <300 nm [5, 6]. The intensity ratio of two bands, I_D/I_G, can be expressed as follows:

$$\frac{I_D}{I_G} = \frac{C(\lambda)}{L_\alpha} \quad (1)$$

where $C(\lambda)$ is 4.4 nm for incident laser wavelengths of 488 and 514 nm [5, 6] and 5.8 nm for an incident laser of 633 nm (Y. Ward, R. J. Young, unpublished results). The position, width and relative intensity ratio of the D- and G-bands determined from Raman spectra in Fig. 1 for all the monofilaments are shown in Table 2. The intensity ratio

Table 2 Raman band positions, bandwidths and ratio of intensities, I_D/I_G, from carbon coatings on the different SiC monofilaments

Monofilaments	Position (cm^{-1})		Width (cm^{-1})		I_D/I_G	L_α (nm)
	D-band	G-band	D-band	G-band		
SCS-6	1321	1580	210	127	1.4	4
Ultra-SCS	1322	1590	150	90	1.1	5
SM1140+	1324	1595	218	110	1.5	4
A	1325	1595	235	110	1.3	4
B	1325	1594	235	110	1.3	4

indicates that the carbon has a typical crystal size of ~4 nm. This is consistent with other microstructural investigations. TEM studies [3, 17, 18] indicate that the carbon is essentially turbostratic, with L_a and L_c of the order of 2–3 nm, roughly aligned with the graphite *c*-axis normal to the monofilament surface [18].

The Raman spectra in Fig. 1 also indicate that the coatings on the monofilaments, SM1140+, samples A and B, are composed of pure carbon without the presence of small SiC particles. This is a direct result of the use of a gas mixture of propane and chloroform in the coating process. Hence the coating axial modulus of these SiC monofilaments is dependent solely on the microstructure of the carbon. The small crystal size, combined with a degree of disorder, leads to a low coating modulus. The axial modulus for the carbon coating on the SM1140+ monofilaments has been determined experimentally to be around 100–120 GPa [1]. An increase in crystallite size or structural order in the carbon structure is correlated with a higher carbon modulus based on the previous work on carbon fibres [10–13].

The coating on the SCS-6 monofilament is different. It has been found [3] (Y. Ward, R. J. Young, unpublished results) that the coating on the SCS-6 is actually a mixture of carbon and SiC, with small SiC crystallites distributed non-uniformly in the carbon structure. This is due to the use of propane and dichlorosilane in the coating process [19]. SiC usually shows characteristic bands between 600 and 1,000 cm^{-1} in the Raman spectrum. However, the Raman scattering efficiency of carbon is about 10 times of that of SiC for an incident laser of 514 nm [20], so the Raman spectrum is not a very sensitive means of detecting SiC in the presence of carbon. It can be observed that the carbon bands dominate the Raman spectra in Fig. 1 making it difficult to detect the presence of SiC in the carbon coating. However, when a longer wavelength laser (785 nm) is used, the SiC Raman bands start to appear in the spectra as shown in the inset to Fig. 1. This inset also shows the Ultra-SCS also has some SiC in the carbon coating, although there appears to be less than in SCS-6.

Strain or stress-dependent Raman band shifts in carbon (graphite)

In order to measure stress or strain in the carbon coating, the dependence of Raman band shifts upon stress or strain is required. For a uniaxial stress σ, applied along the basal plane of the graphite, the stress dependence of the graphite G-band position can be expressed by the following equation [11]:

$$\frac{d\Delta\nu^G}{d\sigma} = \frac{1}{2\nu_0^G}[(A+B)S_{11} + (A-B)S_{12}] \quad (2)$$

In the equation, ν_0^G is the band position of the G-band occurring at 1580 cm^{-1} in the absence of stress. The elastic compliance constants of graphite have been determined as $S_{11} = 0.98 \times 10^{-3}$ GPa^{-1} and $S_{12} = -0.16 \times 10^{-3}$ GPa^{-1} [21]. The material constants A and B describe the changes in the spring constants of the optical phonon modes with strain, and have been determined as $A = -1.44 \times 10^7$ cm^{-2}, and $B = 5.80 \times 10^6$ cm^{-2} [11]. Thus the effect of stress on the shift of the G-band in graphite can be described by

$$\frac{d\Delta\nu^G}{d\sigma} = -1.64\,(cm^{-1}/GPa) \quad (3)$$

This equation indicates that a negative, compressive stress results in an upward shift of the Raman band, whereas a positive tensile stress results in a downshift. Experimentally, the shift of Raman band position with applied strain is easier to determine. Equation 3 is modified to

$$\frac{d\Delta\nu^G}{d\varepsilon} = -1.64E\,(cm^{-1}) \quad (4)$$

i.e., the Raman shift with applied strain is linearly dependent on the modulus of the carbon, E (in GPa).

Figure 2 demonstrates how the positions of both carbon bands change with tensile strain in an SM1140+ monofilament, applied using a four-point bending apparatus as described previously [16]. It shows that the tensile strain causes a linear shift of both carbon bands towards lower wavenumber. The strain-dependent band shifts are found to be –2.6 cm^{-1}/% for the D-band and –1.8 cm^{-1}/% for the G-band. This gives 110 GPa as an estimate for the carbon coating modulus, using Eq. 4, in excellent agreement with previous measurements [1]. A similar experiment on SCS-6 gives –3.6 cm^{-1}/% for the D-band shift and –2.6 cm^{-1}/% for the G-band. This gives an estimate of 160 GPa for the coating modulus of SCS-6 [16].

The higher modulus of the carbon coating in SCS-6 could be due to a slightly larger carbon crystallite size, a higher degree of orientation of the carbon planes parallel to the fibre surface, or the presence of SiC within the structure. If it is assumed that the SiC is responsible, then a

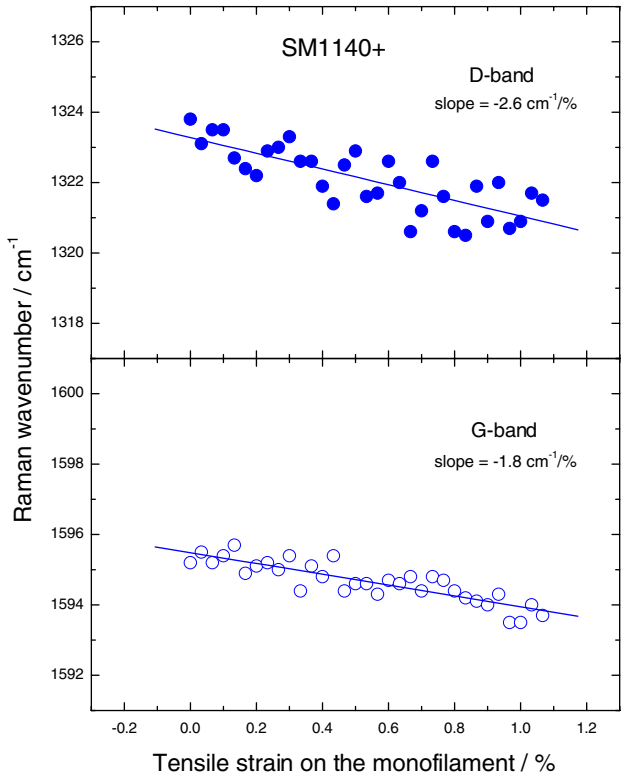

Fig. 2 Shifts in position of carbon D- and G-bands with tensile strains applied on the monofilament SM1140+. The *straight lines* are the linear least-square fits of the data

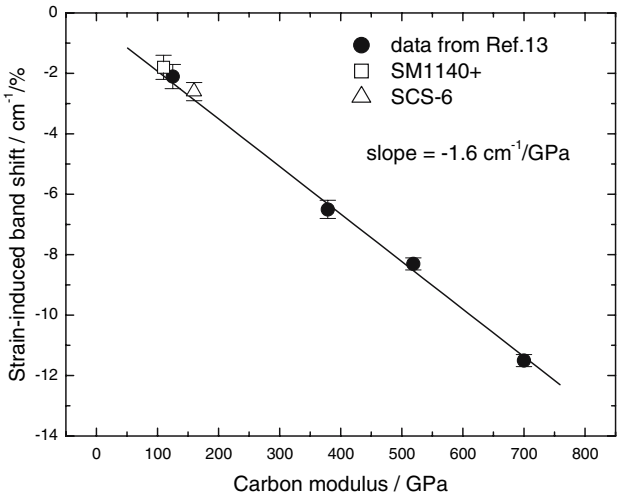

Fig. 3 The strain-induced band shift, $\frac{d\Delta\nu}{d\varepsilon}$ for the carbon G-band is plotted as a function of axial modulus of carbon (carbon fibres data from Ref. [13] and SiC monofilaments SM1140+ and SCS-6 from Ref. [16])

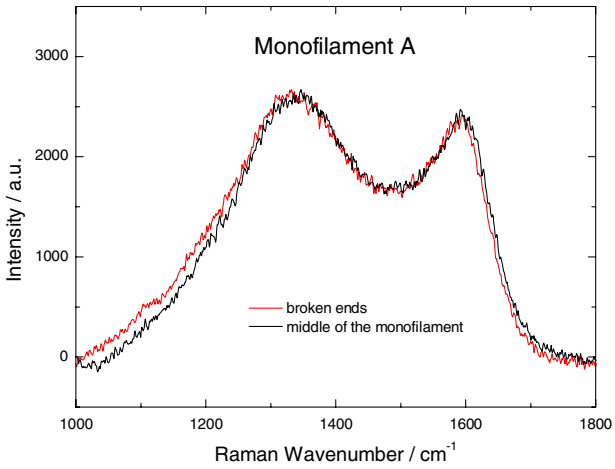

Fig. 4 Raman spectra in the range 1,000–1,800 cm^{-1} obtained from the carbon coating near the broken end and middle of monofilament A

volume fraction calculation, assuming E_C = 110 GPa, E_{SiC} = 420 GPa, indicates that the SCS-6 coating contains around 16% SiC. This is reasonably consistent with the findings of Ning et al. [22].

The strain induced band shifts of these coatings are consistent with those of carbon fibres. Figure 3 demonstrates this, using data from the monofilaments and a variety of carbon fibres.

Residual stresses in the carbon coatings

Raman spectroscopy has been used to determine thermal residual stresses in SiC monofilaments when they are used to reinforce titanium matrix composites [16]. Residual compressive stresses of around –540 MPa were found in the carbon coating of SM1140+, arising from thermal mismatch between the titanium matrix and SiC monofilament. The carbon coating on a free monofilament should also have residual stresses as these coatings are deposited at ~1000 °C. Subsequent cooling to room temperature should lead to compressive axial stresses, as the coefficient of thermal expansion of the partially aligned carbon in the fibre axial direction will be lower than that of SiC. It should be possible to estimate the magnitude of these stresses from Raman measurements. Since the broken end of a monofilament is stress-free, any difference in the band position between the end and middle of a monofilament could be attributed to the residual stresses present in the carbon coatings.

Table 3 Raman band shifts, $d\Delta v$ and corresponding axial residual stresses, in the coatings of different SiC monofilaments

Monofilaments	$d\Delta v$ (cm^{-1})		Residual stress (MPa)
	D-band	G-band	
SCS-6	+1.2(±0.3)	+0.8(±0.3)	–530
Ultra-SCS	+1.8(±0.3)	+1.3(±0.3)	–810
SM1140+	+0.9(±0.5)	+0.7(±0.4)	–440
A	+1.7(±0.4)	+1.2(±0.4)	–750
B	+1.6(±0.4)	+1.1(±0.4)	–690

Figure 4 presents the Raman spectra obtained from the broken end and the middle of monofilament A. It can be observed that both carbon bands from the middle of the monofilaments are shifted towards higher wavenumber, indicating residual compressive stresses in the middle region.

Equation 3 can be used to evaluate the axial stress difference between the ends and middle of the monofilament. The results are shown in Table 3. For each Raman band shift, $d\Delta v$, the mean value and standard deviation obtained from 20 measurements are given. It can be seen that there are significant stresses in the carbon coatings of all SiC monofilaments. The coating stresses in the monofilaments are compressive, with values ranging from –440 MPa in SM1140+ to –810 MPa for Ultra-SCS.

The internal stresses arising from thermal mismatch in the carbon coatings of different SiC monofilaments can be calculated from the continuous coaxial cylinder model of Warwick and Clyne [23]. The parameters used in the coaxial cylinder calculation of internal stresses are shown in Table 4 for SM1140+ and SCS-6. These give the measured coating stresses when used in a coaxial model with a

Table 4 Parameters used in coaxial cylinder model calculations of internal stresses in the carbon coatings of different SiC monofilaments

Material	Outer radius (μm)	Young's modulus (GPa)		Poisson's ratio		CTE ($\times 10^{-6}$ K^{-1})	
		Axial	Radial	Axial	Radial	Axial	Radial
SM1140+							
W	7.5	410	410	0.28	0.28	4.3	4.3
SiC	49	380	380	0.17	0.17	5	5
C	53	110	1	0.23	0.23	0.8	10
SCS-6							
C_{core}	15	390[a]	390	0.17	0.17	5	5
SiC	67	390	390	0.17	0.17	5	5
C	70	160	1	0.23	0.23	1.4	10

[a] The authors have no information on the modulus of the carbon core. However, the stresses in the outer carbon coating are not significantly affected by this parameter, so a nominal value has been assumed

nominal coating deposition temperature of ~1000 °C. The SiC moduli of the monofilaments were measured using techniques described in Ref. [1]. The radial modulus of the carbon coating was estimated using nano-indentation techniques in Ref. [18]. The axial moduli of the carbon coatings used were from this present study. The axial coefficient of thermal expansion (CTE) of the carbon coating was varied to give the compressive coating stresses observed in Table 3, using an estimate for the radial coefficient of thermal expansion (CTE). Whilst the parameters obtained do not represent unique fits to the data, they are reasonable. The axial coating stresses are dependent mostly on the axial coating modulus, coefficient of thermal expansion and deposition temperature. The fits suggest that the inclusion of SiC in the coating of SCS-6 increases both the modulus and coefficient of thermal expansion.

It was not considered appropriate to fit the data on the other monofilaments to the coaxial cylinder model, as

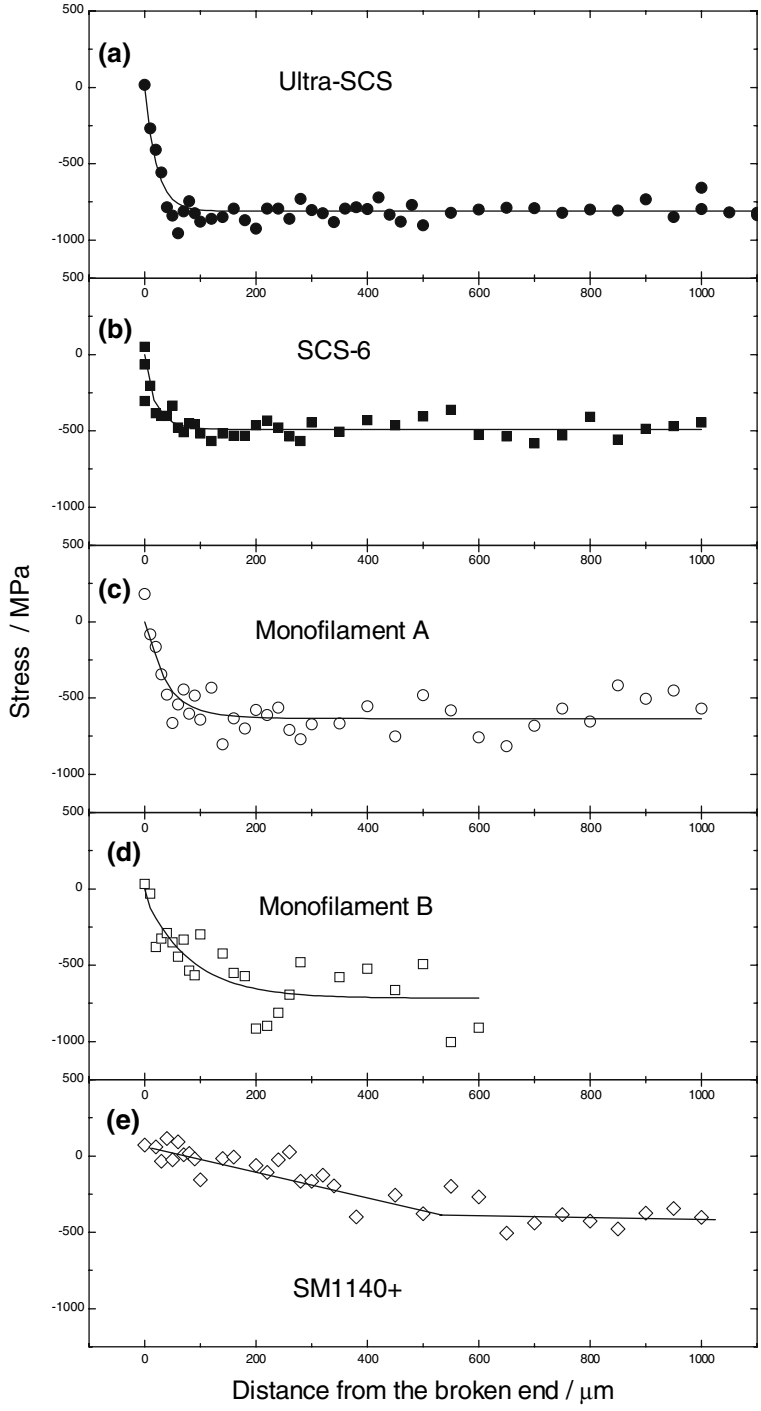

Fig. 5 Stress distribution measured along the axial direction as a function of distance from a broken end for a variety of coated monofilaments. (**a**) Ultra-SCS, (**b**) SCS-6, (**c**) monofilament A, (**d**) monofilament B and (**e**) SM1140

relatively little is known about them. However, Ultra-SCS has higher axial coating stresses despite having less SiC co-deposited with the carbon. This suggests a more graphitic carbon with higher axial modulus and lower CTE than found in SCS-6 or SM1140+.

Axial stress distributions and coating adhesion

Raman spectra were taken at 10–20 μm intervals moving away from the broken ends of the monofilaments. Equation 3 was used to compute the stress difference between the measurement position and the monofilament end. The results are shown in Fig. 5(a)–(e). All samples show a build up of compressive coating stress with distance, but there are significant differences between the different monofilaments. The stress build-up in Ultra-SCS takes place over ~50 μm, whereas SM1140+ shows a slow build-up of stress well over ~500 μm. Both monofilaments A and B, show the stress build-up over the distance of ~200 μm. The coatings on monofilaments A and B were deposited in a sequence of experiments seeking to increase the degree of adhesion with the substrate SiC. It was therefore expected that stress build-up would take place in a shorter distance than for SM1140+. In Fig. 5(a)–(d), the data can be fitted to the following function, similar to that described by the shear-lag model used in composite micromechanics [24]:

$$\sigma_x = \sigma_\infty\{1 - \exp(-\beta x)\} \quad (5)$$

where σ_x is the stress in the coating at a distance x from the broken end. This suggests the carbon coating is strongly bonded to the substrate SiC and the stress transfer at the interface is mainly by elastic shear. In contrast, Fig. 5(e) shows a linear build up of compressive stress over a distance of ~500 μm in the coating of SM1140+. This suggests the coating is de-bonded from the underlying SiC and stress transfer takes place via frictional shear. Measurements on a second sample of SCS-6 (not shown) showed zero coating stress along the entire length of the coating. It is suggested that the carbon coating in this case had also de-bonded from the substrate. Since SCS-6 is smoother than SM1140+, frictional transfer of stress did not occur to a measurable extent. It has been observed by one of the authors (RAS) that de-bonding of the coating can occur on fracture of both SCS-6 and SM1140+, in an apparently random manner. It is therefore no surprise that two samples of a similar material show different behaviour. By contrast, the coating on Ultra-SCS always appeared to be well bonded to the substrate after fracture, suggesting a stronger bond. A weak interface is considered beneficial when the fibres are embedded in a composite, so it is possible that optimal properties may not be obtained for composites made with Ultra-SCS.

Conclusions

Raman spectroscopy has been used to study the internal stresses in the carbon coatings of a variety of monofilaments by determining the variations of the band positions with distance from free fibre ends. The axial stress in the coatings of all the monofilaments studied was found to be compressive, consistent with the origin of this behaviour being a thermal mismatch arising from the coefficient of thermal expansion of SiC being greater than that of the carbon coating. The rate of stress build-up away from the monofilament end is significantly different for different monofilaments, being the highest for Ultra-SCS and lowest for SM1140+. This suggests the shear stress at the interface between the carbon coating and underlying SiC is highest for Ultra-SCS.

Acknowledgement The authors would like to thank for the financial support from the EPSRC Platform Program, GR/S19752/01.

References

1. Shatwell RA (1994) Mater Sci Technol 10:552
2. Warwick CM, Kieschke RR, Clyne TW (1991) Acta Met Mater 39:437
3. Ning XJ, Pirouz P (1991) J Mater Res 6:2234
4. Ward Y, Young RJ, Shatwell RA (2001) J Mater Sci 36:55. DOI: 10.1023/A:1004830505979
5. Tuinstra F, Koenig JL (1970) J Chem Phys 53:1126
6. Knight DS, White WB (1989) J Mater Res 4:385
7. Pocsik I, Hundhausen M, Koos M, Ley L (1998) J Non-Cryst Solids 1083:227–230
8. Ferrari AC, Robertson J (2000) Phys Rev B 61:14095
9. Ferrari AC, Robertson J (2001) Phys Rev B 64:075414
10. Chien C, Dresselhaus G, Endo M (1982) Phys Rev B 26:5867
11. Sakata H, Dresselhaus G, Dresselhaus MS, Endo M (1988) J Appl Phys 63:2769
12. Robinson IM, Zakikhani M, Day RJ, Young RJ (1987) J Mater Sci-Lett 6:1212
13. Huang Y, Young RJ (1995) Carbon 33:97
14. Gouadec, Karlin S, Colomban Ph (1998) Compos B 29:251
15. Young RJ, Broadbridge A, So SL (1999) J Microsc 196:257
16. Ward Y, Young RJ, Shatwell RA (2002) Compos A 33:1409
17. Cheng TT, Jones IP, Shatwell RA, Doorbar P (1999) Mater Sci Eng A260:139
18. Kendig KL (1999) PhD Thesis, University of Michigan
19. DeBolt HE, Suplinskas RJ, Cornie JA, Henze TW, Hauze AW (1982) US Patent 4340636
20. Sasaki Y, Nishina Y, Sato M, Okamura K (1987) J Mater Sci 22:443. DOI: 10.1007/BF01160751
21. Kelly BT (1981) Physics of graphite. Applied Science, London
22. Ning XJ, Pirouz P, Farmer SC (1993) J Am Chem Soc 76:2033
23. Warwick M, Clyne TW (1991) J Mater Sci 26:3817. DOI: 10.1007/BF01184978
24. Kelly A, Macmillan NH (1986) Strong solids, 3rd edn. Clarendon Press, Oxford